Journal of Quantitative Spectroscopy & Radiative Transfer 110 (2009) 1604–1614

Contents lists available at ScienceDirect

Journal of Quantitative Spectroscopy & Radiative Transfer

journal homepage: www.elsevier.com/locate/jqsrt

Dependence of ice crystal optical properties on particle aspect ratio

Ping Yang [a,*], Qiang Fu [b]

[a] Department of Atmospheric Sciences, Texas A&M University, College Station, TX 77843, USA
[b] Department of Atmospheric Sciences, University of Washington, Seattle, WA 98195, USA

ARTICLE INFO

Article history:
Received 7 January 2009
Received in revised form
1 March 2009
Accepted 5 March 2009

Keywords:
Ice crystals
Asymmetry factor
Aspect ratio

ABSTRACT

The single-scattering properties of randomly oriented hexagonal ice crystals have been extensively used to study the bulk radiative properties of ice clouds. It has been reported in the literature that the asymmetry factors of these particles vary with their aspect ratios in a "V-pattern" with the minimum at a unit aspect ratio. However, this phenomenon was not explained in the previous studies. The present paper reports on an in-depth analysis of the optical properties of hexagonal ice crystals. It is shown that the delta-transmission is primarily responsible for the aforementioned "V-pattern" variation of the asymmetry factor as a function of the aspect ratio. Additionally, the term $(1-f_\delta)g$ is also partially responsible for the large values of the total asymmetry factor in the case of small aspect ratios, where f_δ indicates the ratio of the amount of the energy associated with the delta-transmission rays to the total amount of the scattered energy and g is the asymmetry factor associated with the geometric optics rays.

1. Introduction

It is generally recognized that ice clouds are one of the highly uncertain climate components in quantitative climate studies. To improve our knowledge of the role of ice clouds in the energy budget of the earth-atmosphere system, considerable effort has been made in the past three decades to better understand the radiative effect and microphysical and optical properties of these clouds [1–7]. Particularly, a number of parameterization schemes for the bulk radiative properties of ice clouds, which are based on the optical properties of individual ice crystals, have been developed for applications to general climate models (GCMs). Although complex particle geometries, such as bullet rosettes, aggregates and polycrystals, have been considered in some parameterizations (e.g., [8,9]), several schemes [10–12] are based on the single-scattering properties of hexagonal ice crystals. Using ice water content and generalized effective size that conserves both total volume and projected area of nonspherical ice particles, a hexagonal-geometry-based scheme for parameterizing the extinction coefficient and single-scattering albedo can be a good approximation for applications to studying the radiative properties of cirrus clouds consisting of various nonspherical particles such as plates, columns, bullet rosettes, and aggregates. Recently, Fu [13] introduced a mean effective aspect ratio for an ensemble of ice crystals to generalize the applicability of the hexagonal-geometry-based parameterization of the asymmetry factor associated with the scattering of solar radiation by cirrus clouds.

Neshyba et al. [14], Grenfell et al. [15] and Fu [13] showed that the variation of the asymmetry factors for individual hexagonal ice crystals versus their aspect ratios presents a "V-pattern" as the aspect ratios vary from those for columns to their counterparts for plates. The minimum asymmetry factor occurs approximately at a unit aspect ratio. This interesting

* Corresponding author. Tel.: +1 979 845 4923.
E-mail address: pyang@ariel.met.tamu.edu (P. Yang).

0022-4073/$ - see front matter © 2009 Elsevier Ltd. All rights reserved.
doi:10.1016/j.jqsrt.2009.03.004

scattering feature, however, has not been explained from the perspective of a fundamental scattering process within the framework of the geometric optics method, although the scattering properties of hexagonal ice crystals have been extensively investigated [16–26]. This study is intended to provide an in-depth analysis of the dependence of the single-scattering properties of hexagonal ice crystals on their aspect ratios; particularly, an explanation of the aforementioned "V-pattern" variation of the asymmetry factor versus the aspect ratio is presented.

2. Geometric optics solution for the optical properties of ice crystals

The present study is limited to the optical properties of hexagonal ice crystals. Note that a comprehensive database of the single-scattering properties of hexagonal ice crystals has been developed by Hess and Wiegner [19]. Hexagonal geometry is the basic structure of ice crystals although it has been suggested that pristine hexagonal plates and columns are rare in cirrus clouds because halos are not often observed [27]. The physical dimension of a hexagonal ice crystal can be specified in terms of its length (L) and cross section width (D), which are indicated in panels (a) and (b) in Fig. 1, respectively. The aspect ratio (α) of the particle is defined in the form

$$\alpha = D/L. \tag{1}$$

The sizes of most ice crystals within cirrus clouds are on the order of several tens and hundreds of microns, and, thus, the corresponding size parameters in the solar spectral region are in the geometric optics regime. For this reason, we use the conventional ray-tracing technique to compute the single-scattering properties of hexagonal ice crystals. The technical details of the ray-tracing method are not reiterated here because they were thoroughly described in several previous studies (e.g., [16–18,20,21,25]). In this study, the scattered rays are categorized into different orders according to their histories. The zero-order scattered field is for the diffraction of the incident wave, which can be computed from a formula presented by Yang and Liou [26] for the entire 0°–180° scattering region. Note that the conventional diffraction formulation [16] can be applied only to the scattering angles ranging from 0° to 90°. As shown in panel (c) of Fig. 1, the first-order ($n = 1$) rays indicate externally reflected rays, the second-order ($n = 2$) rays indicate those that undergo two sequential refractions without undergoing an internal reflection, and the third-order ($n = 3$) rays indicate those that undergo one internal reflection and two refractions. The scattered field is the sum of the contributions from diffraction and geometric optics rays with orders from $n = 0$ to N. In theory, N is infinite; however, it is sufficient to only consider the rays of orders with $n < 14$ because the energy associated with the rays of higher orders is negligible.

An outcome inherent to the ray-tracing method is the delta-transmission associated with the collimated rays that transmit through two parallel faces of an ice crystal and propagate along the incident direction. Panel (d) in Fig. 1

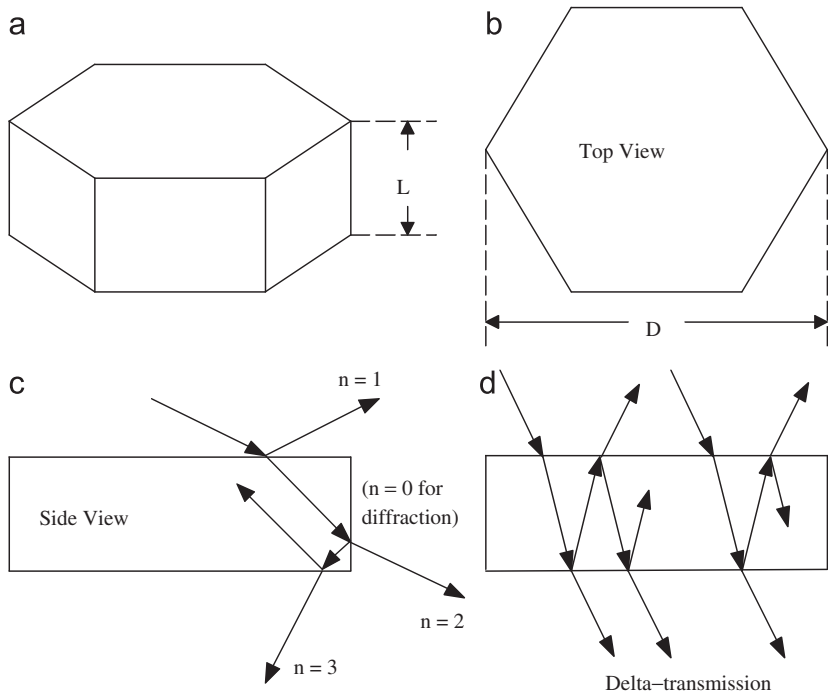

Fig. 1. (a) and (b) The geometry of a hexagonal ice plate. (c) Geometric optics rays of different orders. Note that $n = 0$ indicates the contribution from diffraction (not shown in the diagram). (d) Schematic illustration of the delta-transmission rays.

schematically illustrates the delta-transmission. The proper treatment of the delta-transmission in the ray-tracing calculation has been discussed in detail by Takano and Liou [17] and Mishchenko and Macke [28].

The scattering phase matrix of an ensemble of randomly oriented ice crystals, which include the contribution of the delta-transmission, can be written in the form

$$\tilde{P}(\theta)=2f_\delta\delta(\cos\,\theta-1)\begin{bmatrix}1&0&0&0\\0&1&0&0\\0&0&1&0\\0&0&0&1\end{bmatrix}+(1-f_\delta)\begin{bmatrix}P_{11}(\theta)&P_{12}(\theta)&0&0\\P_{12}(\theta)&P_{22}(\theta)&0&0\\0&0&P_{33}(\theta)&-P_{43}(\theta)\\0&0&P_{43}(\theta)&P_{44}(\theta)\end{bmatrix}. \tag{2}$$

In Eq. (2), the term f_δ indicates the ratio of the amount of the energy associated with the delta-transmission rays to the total amount of the scattered energy. The phase matrix $\tilde{P}(\theta)$ has only six independent nonzero elements because of the randomly orientations of the scattering particles [29]. In Eq. (2), the term $P_{11}\,(\theta)$ is normalized in the form

$$\frac{1}{2}\int_0^\pi P_{11}(\theta)\sin\,\theta\,d\theta=1. \tag{3}$$

The second term on the right-hand side of Eq. (2) can be decomposed into the contributions from diffraction and the geometric optics rays. The latter can be further expressed in terms of the contributions of the rays of different orders excluding the delta-transmission component. Thus, we have

$$\begin{aligned}\begin{bmatrix}P_{11}(\theta)&P_{12}(\theta)&0&0\\P_{12}(\theta)&P_{22}(\theta)&0&0\\0&0&P_{33}(\theta)&-P_{43}(\theta)\\0&0&P_{43}(\theta)&P_{44}(\theta)\end{bmatrix}&=\frac{0.5}{\tilde{\omega}(1-f_\delta)}\begin{bmatrix}P_{11}^d(\theta)&P_{12}^d(\theta)&0&0\\P_{12}^d(\theta)&P_{22}^d(\theta)&0&0\\0&0&P_{33}^d(\theta)&0\\0&0&0&P_{33}^d(\theta)\end{bmatrix}\\&+\frac{\tilde{\omega}-\tilde{\omega}f_\delta-0.5}{\tilde{\omega}(1-f_\delta)}\begin{bmatrix}P_{11}^{r,t}(\theta)&P_{12}^{r,t}(\theta)&0&0\\P_{12}^{r,t}(\theta)&P_{22}^{r,t}(\theta)&0&0\\0&0&P_{33}^{r,t}(\theta)&-P_{43}^{r,t}(\theta)\\0&0&P_{43}^{r,t}(\theta)&P_{44}^{r,t}(\theta)\end{bmatrix}\\&=\sum_{n=0}^{N}\begin{bmatrix}P_{11}^{(n)}(\theta)&P_{12}^{(n)}(\theta)&0&0\\P_{12}^{(n)}(\theta)&P_{22}^{(n)}(\theta)&0&0\\0&0&P_{33}^{(n)}(\theta)&-P_{43}^{(n)}(\theta)\\0&0&P_{43}^{(n)}(\theta)&P_{44}^{(n)}(\theta)\end{bmatrix}.\end{aligned} \tag{5}$$

In Eq. (5), the superscript *d* indicates diffraction contribution whereas the superscript *r,t* indicates the contribution from the geometric optics rays excluding the delta-transmission. P_{11}^d and $P_{11}^{r,t}$ are normalized. The term $\tilde{\omega}$ indicates the single-scattering albedo. In the calculation of $\tilde{\omega}$, the delta-transmission rays are regarded as scattered rays although they are collimated rays propagating along the incident direction.

The asymmetry factor associated with the scattering phase function can be expressed as follows:

$$\begin{aligned}\tilde{g}&=\frac{1}{2}\int_0^\pi\tilde{P}_{11}(\theta)\cos\,\theta\,\sin\,\theta\,d\theta\\&=f_\delta+(1-f_\delta)g\\&=f_\delta+(1-f_\delta)\left[\frac{0.5}{\tilde{\omega}(1-f_\delta)}g^d+\frac{\tilde{\omega}-\tilde{\omega}f_\delta-0.5}{\tilde{\omega}(1-f_\delta)}g^{r,t}\right]\\&=f_\delta+(1-f_\delta)\sum_{n=0}^{N}g^{(n)},\end{aligned} \tag{6}$$

where $g, g^d, g^{r,t}$, and $g^{(n)}$ are associated with $p_{11}, p_{11}^d, p_{11}^{r,t}$, and $p_{11}^{(n)}$, respectively. Because the scattered energy associated with diffraction is concentrated in a narrow angular region around the forward direction ($\theta=0^\circ$), particularly, in the case of large ice crystals, g^d is essentially unity. Note that Fu [13] approximated the asymmetry factor using different notations as follows (see Eq. (2.2) in Ref. [13]):

$$g=\frac{1}{2\tilde{\omega}}+\left[1-\frac{1}{2\tilde{\omega}}\right]g'. \tag{7}$$

The parameter g in Eq. (7) is essentially the same as $\tilde{g}$ defined in the present study. In Eq. (7), the asymmetry factor associated with diffraction, g^d, is assumed to be 1. It is evident from a comparison of Eqs. (6) and (7) that the parameter g' in

Eq. (7) is the same as $g^{r,t}+2\tilde{\omega}f_\delta(1-g^{r,t})(2\tilde{\omega}-1)^{-1}$. Furthermore, the term g' in Eq. (7) includes the contribution of the delta-transmission.

3. Results and discussions

Fig. 2 shows the contributions of the rays of various orders to the scattering phase matrix of randomly oriented hexagonal compact (i.e., the aspect ratio $\alpha=1$) ice crystals with a size of $D/L=300\,\mu m/300\,\mu m$ at a visible wavelength of 0.55 μm. Cai and Liou [16] reported a similar result but for randomly oriented hexagonal columns with the incident direction normal to the symmetry axis of the particle. Hess et al. [30] reported the contributions of successive orders of geometric optics rays to the scattering phase matrix of randomly oriented imperfect hexagonal ice crystals. However, in the previous studies the phase functions were normalized when the contributions from the geometric optics rays were sequentially added up, and, thus, the relative weights of the contributions from the rays of various orders cannot be determined from their results (Fig. 6 in Ref. [16] and Fig. 6 in Ref. [30]).

It is evident from Fig. 2 that the contribution from diffraction and external reflection to the phase function is featureless, except for a strong forward peak associated with the diffracted energy in the forward direction. The two peaks at 22° and 46° are attributed to the contribution of the rays when $n=2$ with a mechanism that is explained in many classic texts (e.g., Liou [31]). For the scattering angles from 0° to 115°, the contributions from the rays of the first four orders (i.e., $n=0$, 1, 2 and 3) dominate. However, at the scattering angles ranging from 115° to 180° the rays with orders higher than 3, have significant contributions. Similarly, it can be seen from the results for other phase matrix elements that the major polarizations features are from the first four orders of the rays at the scattering angles ranging from 0° to 115°. At the scattering angles larger than 115°, it is important to account for higher order ($n>3$) rays. Furthermore, it is critical to account for the contributions from the rays with orders higher than 5 in the case of P_{43}/P_{11} and P_{44}/P_{11} although the first five orders ($n=0,1,2\ldots4$) of the rays almost give converged solutions for $-P_{12}/P_{11}, P_{22}/P_{11}$ and P_{33}/P_{11}. The asymmetry factor $\tilde{g}$ and delta transmission factor f_δ for the phase function $\tilde{P}$ corresponding to the results in Fig. 2 are 0.7398 and 0.1208, respectively.

Figs. 3 and 4 are similar to Fig. 2, except for long columns and thin plates, respectively. To have the same magnitude of diffraction peaks, we have defined the projected areas of randomly oriented ice crystals, given by $(3/4)L^2\alpha[1+(\sqrt{3}/4)\alpha]$, to be the same for Figs. 2–4. The asymmetry factor $\tilde{g}$ and delta transmission factor f_δ are 0.8664 and 0.1836, respectively, for

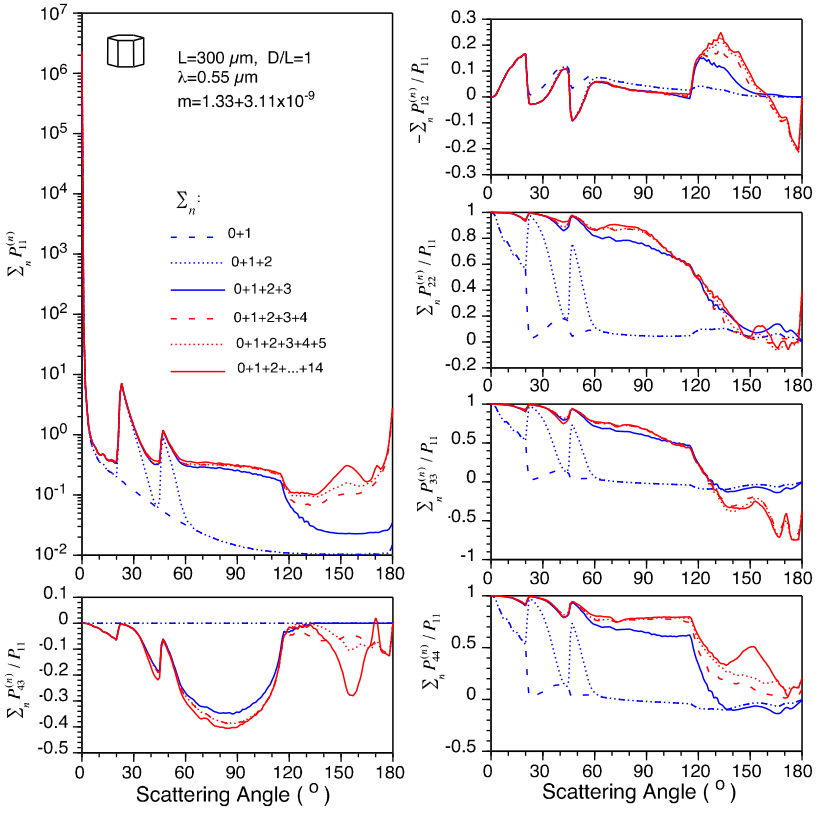

Fig. 2. The contributions of the rays of various orders to the independent nonzero elements of the normalized phase matrix (excluding the delta-transmission) for randomly oriented compact (i.e., $\alpha=1$) hexagonal ice crystals at a visible wavelength of 0.55 μm.

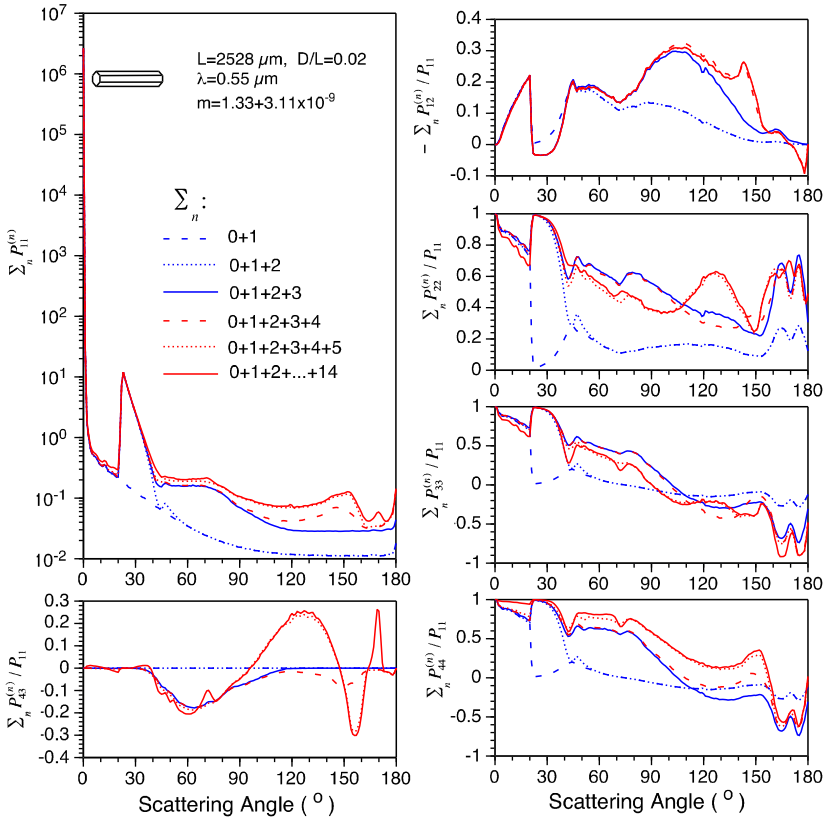

Fig. 3. The contributions of the rays of various orders to the independent nonzero elements of the phase matrix for randomly oriented long (i.e., $\alpha = 0.02$) hexagonal ice columns at a visible wavelength of 0.55 μm.

the long columns shown in Fig. 3, and 0.9413 and 0.4332, respectively, for the thin plates shown in Fig. 4. Evidently, the delta-transmission is quite pronounced in the case of plates because of a significant amount of energy associated with the transmission of rays from a basal face to the other basal face of a hexagonal ice crystal.

The general scattering features shown in Figs. 3 and 4 are similar to those shown in Fig. 2. However, in the case of the long columns shown in Fig. 3, the phase function ($\sum_n : 0+1+2+\cdots+14$) shows a pronounced 22° peak, whereas the 46° scattering peak is effectively not observed. This is because the areas of the basal faces are much smaller than the areas of side faces of the particles so that the energy associated with the refraction from basal to side faces (or vice versa) is insignificant. For long columns, the rays with orders higher than 3 are more important than those for compact ice crystals, as is evident from a comparison between Figs. 2 and 3.

In the case of thin plates shown in Fig. 4, the contributions of the rays of the first four orders (i.e., $\sum_n : 0+1+2+3$) dominate the scattered field, except in a narrow region of scattering angles close to 180°. The phase functions shown in Fig. 4 are relatively featureless in comparison with those shown in Fig. 3, and particularly, the two halo peaks are quite small.

The upper left panel of Fig. 5 shows $\tilde{g}$ as a function of the aspect ratio, where the decomposition of $\tilde{g}$ into two components, $(1-f_\delta)g$ and f_δ, are also shown. Evidently, the "V-pattern" variation of $\tilde{g}$ versus the aspect ratio stems primarily from the dependence of f_δ on the aspect ratio. For the results shown in Fig. 5, the mean projected area of randomly oriented ice crystals is defined to be the same as that of ice crystals with sizes of D/L = 300 μm/300 μm when the aspect ratio varies. The contribution of the diffraction and geometric optics rays (without the inclusion of the delta-transmission rays) to $\tilde{g}$ monotonically increases with the decrease of the aspect ratio and plays a role in defining the "V-pattern". In the case of plates, the delta-transmission is quite significant and can be large, as much as 0.4 for extremely thin plates (D/L∼100). The upper right panel of Fig. 5 shows the variation of $(1-f_\delta)\sum_n g^{(n)}$ versus the aspect ratio. It is shown that the rays with an order of $n=3$ have a significant contribution to $(1-f_\delta)\sum_n g^{(n)}$ when D/L<10. For thin plates (D/L>10), the delta-transmission is significant, and, thus, the diffraction and external reflection dominate the portion of the scattered field that does not include the delta-transmission. The lower panels of Fig. 5 are similar to the upper panels except that they are computed at a wavelength of 2.13 μm at which ice is absorptive. The variation patterns of $\tilde{g}$ and f_δ are similar at the two wavelengths. However, $(1-f_\delta)g$ and $(1-f_\delta)\sum_n g^{(n)}$ have their maxima at D/L∼1.

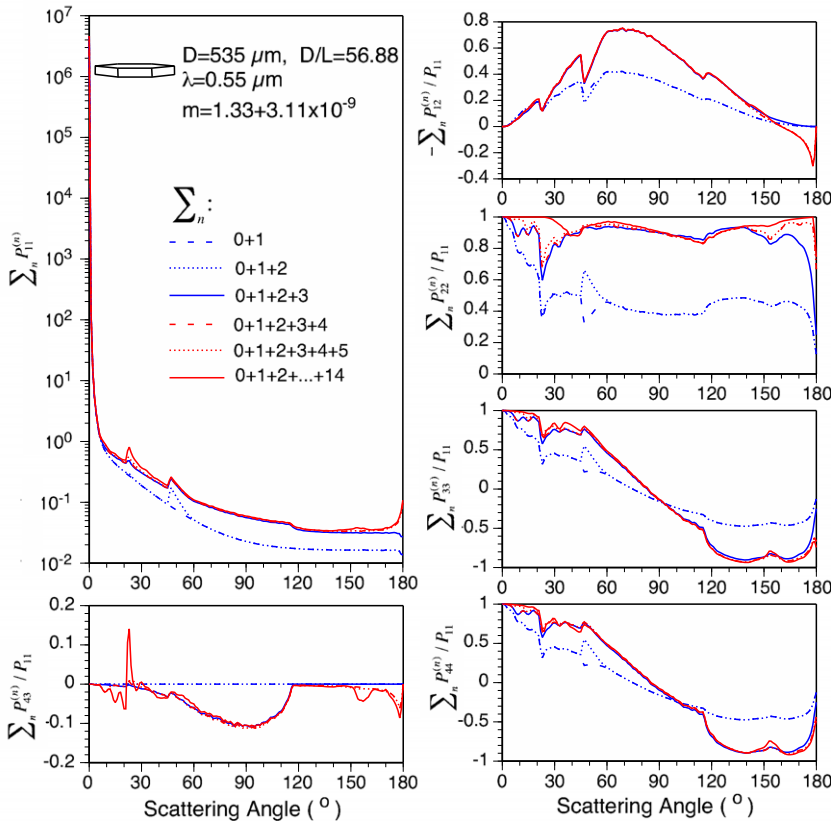

Fig. 4. The contributions of the rays of various orders to the independent nonzero elements of the phase matrix for randomly oriented thin (i.e., $\alpha = 56.88$) hexagonal ice plates at a visible wavelength of 0.55 μm.

Fig. 6 shows $\sum_n g^{(n)}$ as functions of the aspect ratio at wavelengths 0.55 and 2.13 μm. At the 0.55 μm wavelength, the "V-pattern" observed for the variation of $\tilde{g}$ versus the aspect ratio is also observed in the case of $\sum_n g^{(n)}$. However, the "V-pattern" is not pronounced at the 2.13 μm wavelength because of the absorption of ice crystals. It is now clear that the delta-transmission is primarily responsible for the "V-pattern" of the variation of the asymmetry factor $\tilde{g}$ versus the aspect ratio, as evident from Fig. 5.

To understand the physical mechanism, we consider the scattering of light by randomly oriented 2D rectangular particles. The size of a 2D rectangular particle is specified by the lengths of two adjacent sides, a and b, as shown in Fig. 7. Note that, if the particle projected area (a line segment in the 2D case) is conserved, the scattering properties for an aspect ratio of $a/b \geqslant 1/x$ (here x is an arbitrary number) are the same as those for an aspect ratio of $a/b = x$. As shown in Fig. 7, there are three types of direct ray-transmission in the ray-tracing calculation involving a 2D rectangular particle. Type (i) ray-transmission is from a side face to a basal face whereas type (iii) is the opposite. Both type (i) and (iii) rays do not contribute to the delta-transmission. Type (ii) ray-transmission is from a basal face to the other basal face, and is directly responsible for the delta-transmission. The portion of the energy associated with type (ii) rays is the minimum when $a/b = 1$, and thus, the asymmetry factor $\tilde{g}$ is the minimum in this case.

In the 2D case, the scattered intensity associated with an unpolarized incident light beam can be expressed in terms of the 2D phase function as follows:

$$I_s = \frac{\sigma_s}{2\pi r}\tilde{P}_{11}(\varphi) I_0, \tag{8}$$

where the phase function is normalized as follows:

$$\frac{1}{\pi}\int_0^{\pi} \tilde{P}_{11}(\varphi)\, d\varphi = 1. \tag{9}$$

The asymmetry factor can be expressed in the form

$$\tilde{g} = \frac{1}{\pi}\int_0^{\pi} \tilde{P}_{11}(\varphi) \cos\,\varphi\, d\varphi. \tag{10}$$

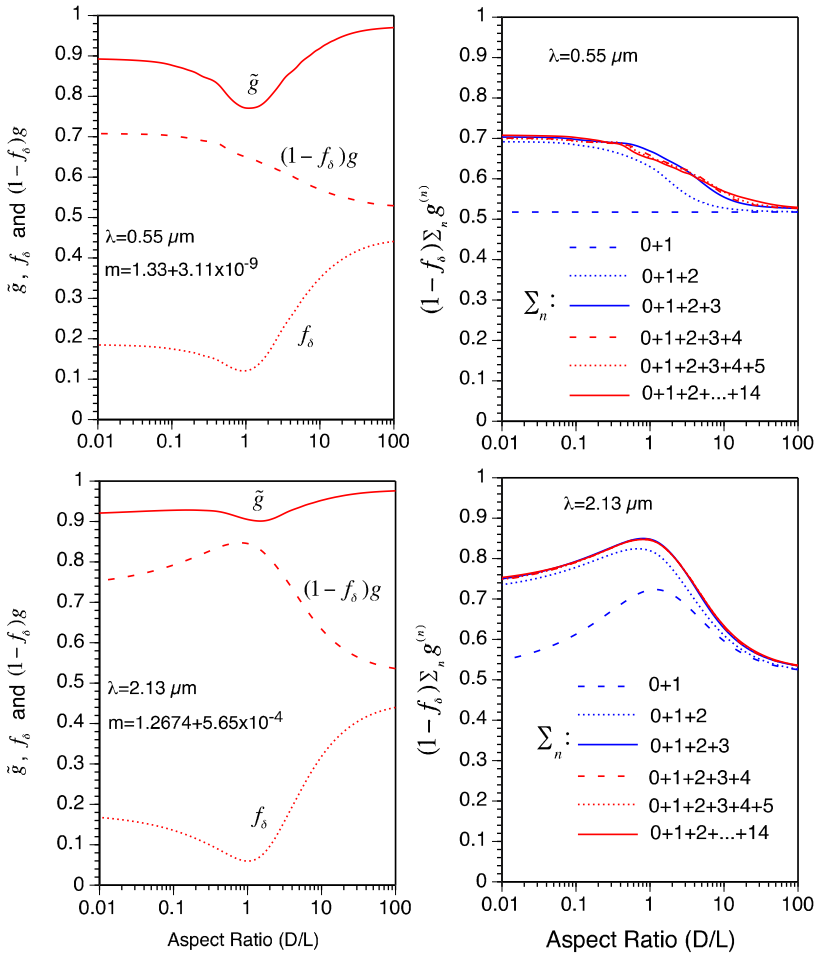

Fig. 5. Variations of $\tilde{g}, f_\delta$, $(1-f_\delta)g$, and $(1-f_\delta)\sum_n g^{(n)}$ as functions of the aspect ratio D/L at wavelengths 0.55 and 2.13 μm.

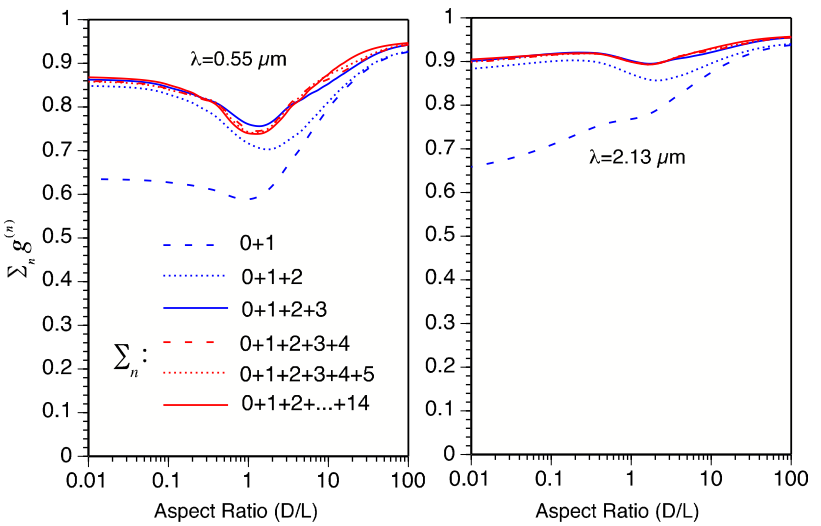

Fig. 6. Variations of $g=\sum_n g^{(n)}$ as functions of the aspect ratio D/L at wavelengths 0.55 and 2.13 μm.

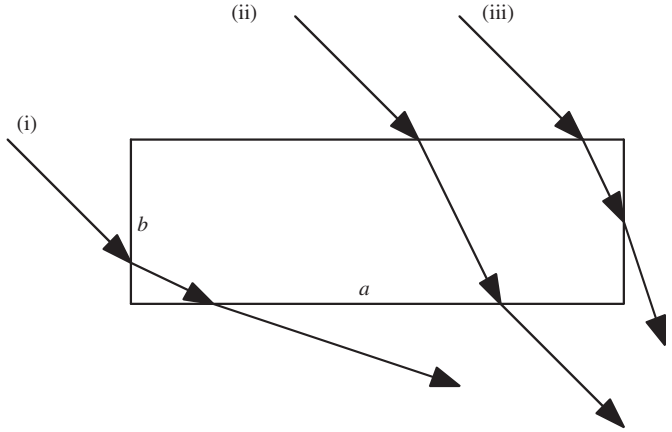

Fig. 7. The transmission of incident rays for the scattering of light by a 2D rectangular particle.

Similar to the 3D phase function, the 2D phase function can be expressed in the form

$$\tilde{P}_{11}(\varphi) = 2f_\delta\delta(\varphi) + (1-f_\delta)P_{11}(\varphi), \tag{11a}$$

$$P_{11}(\varphi) = \frac{0.5}{\tilde{\omega}(1-f_\delta)}P_{11}^{d}(\varphi) + \left[1 - \frac{0.5}{\tilde{\omega}(1-f_\delta)}\right]P_{11}^{r,t}(\varphi), \tag{11b}$$

where $P_{11}(\varphi)$ is normalized. The term $P_{11}^{d}(\varphi)$ is given in the form

$$P_{11}^{d}(\varphi) = \frac{\pi P_{11}^{d'}(\varphi)}{\int_0^\pi P_{11}^{d'}(\varphi)d\varphi}, \tag{12a}$$

$$P_{11}^{d'}(\varphi) = \int_0^{\pi/2}\left\{\frac{kl(\varphi_i)\sin[kl(\varphi_i)\sin\varphi]}{kl(\varphi_i)\sin\varphi}(1+\cos\varphi)\right\}^2 d\varphi_i \tag{12b}$$

$$l(\varphi_i) = (a\cos\varphi_i + b\sin\varphi_i)/2. \tag{12c}$$

Fig. 8 shows the phase functions associated with the scattering of light by randomly oriented 2D rectangular particles for four aspect ratios, $a/b = 1, 5, 10$, and 100. The particle projected area is defined as the same as that in the case of $a/b = 50\,\mu m/50\,\mu m$. The incident electric vector is assumed to be normal to the 2D particle (i.e., perpendicular to the paper). The 46° peak in the phase function is associated with the so-called minimum deviation of the rays transmitted through two adjacent sides, which is insignificant for an extreme aspect ratio, i.e., $a/b = 100$. It is evident from the parameters listed in Fig. 8 that the delta-transmission increases with the increase of the aspect ratio. In the case of $a/b = 100$, the scattering particle is similar to a thin plate for which a significant portion of the incident energy is directly transmitted through and continues to propagate in the original direction after the transmission.

Fig. 9 shows the variations of $\tilde{g}$, $(1-f_\delta)g$ and f_δ for the 2D rectangular particles. Similar to the 3D case shown in Fig. 5, the curves of $\tilde{g}$ and f_δ show minima at $a/b = 1$. The symmetric pattern of the variations of $\tilde{g}$, $(1-f_\delta)g$ and f_δ are evident from Fig. 9. The contribution from the geometric optics rays to the asymmetry factor, i.e., the $(1-f_\delta)g$ component of $\tilde{g}$, does not strongly depend on the aspect ratio. Similar to the 3D case shown in Fig. 5, the 2D case shown in Fig. 9 also illustrates that the "V-pattern" of the variation of $\tilde{g}$ versus the aspect ratio is due to the dependence of the delta-transmission.

The polarization state of the backscattered light contains rich information for active remote sensing applications. Fig. 10 shows the contributions of various orders of rays to the backscattering depolarization ratio associated with 3D randomly oriented hexagonal ice columns and plates, which is defined in the form

$$\delta^{(n)} = \frac{1 - \sum_n P_{22}^{(n)}/P_{11}}{1 + \sum_n P_{22}^{(n)}/P_{11}}. \tag{13}$$

It is evident from Fig. 10 that the depolarization ratio pattern as a function of the aspect ratio is quite different for plates and columns. For plates with aspect ratios between 1 and 10, the depolarization ratios show oscillations, which are associated with high orders of rays. Unlike the case for the asymmetry factor, the depolarization ratio as a function of the aspect ratio reaches its maximum when the aspect ratio is approximately 0.1. Furthermore, the depolarization ratios for plates are smaller than those for columns.

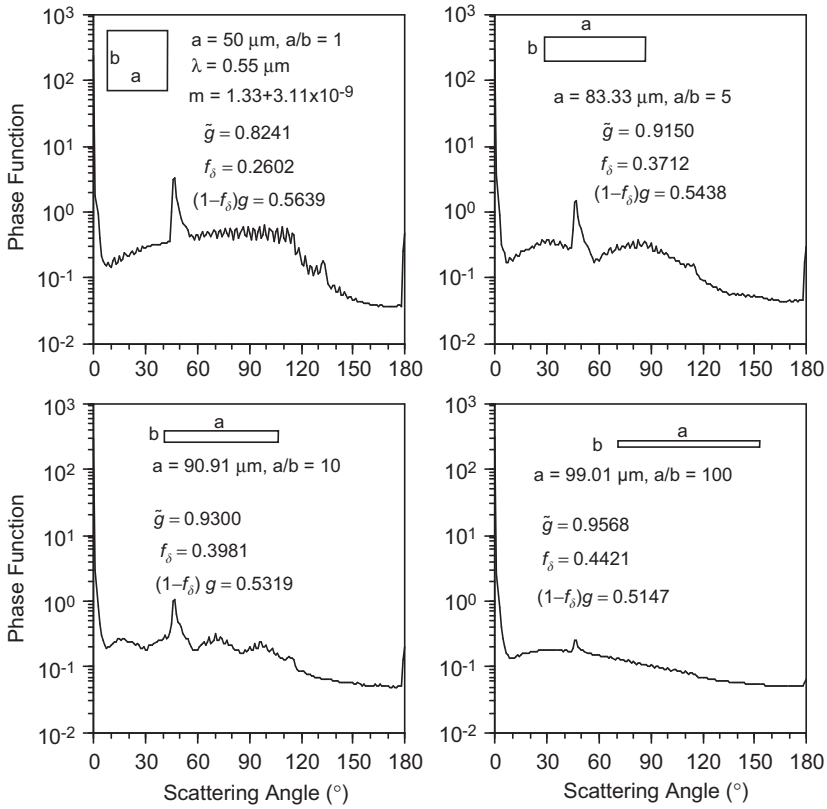

Fig. 8. The phase functions of randomly oriented 2D rectangular particles for four aspect ratios, $a/b = 1$, 5, 10 and 100. Note that the projected line of the particle is defined the same as that of a particle with a size of $a/b = 50\,\mu m/50\,\mu m$.

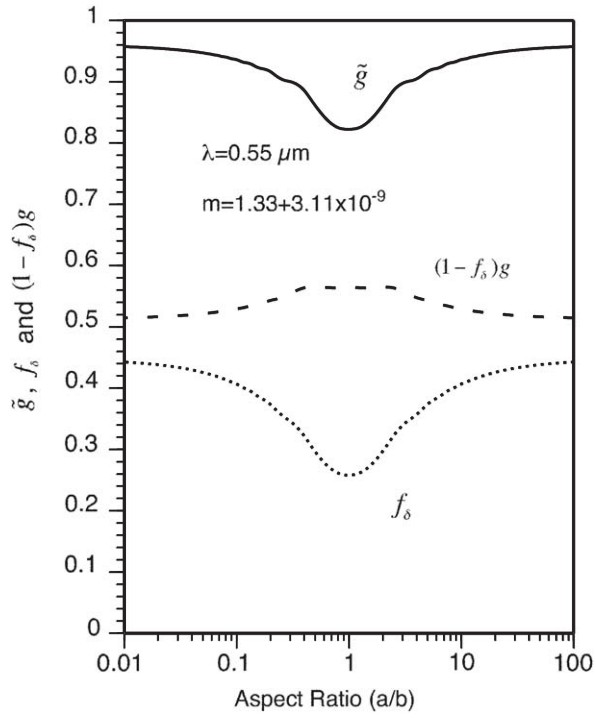

Fig. 9. Variations of $\tilde{g}$, f_δ, $(1-f_\delta)g$, and $(1-f_\delta)\sum_n g^{(n)}$ as functions of the aspect ratio for 2D rectangular particles.

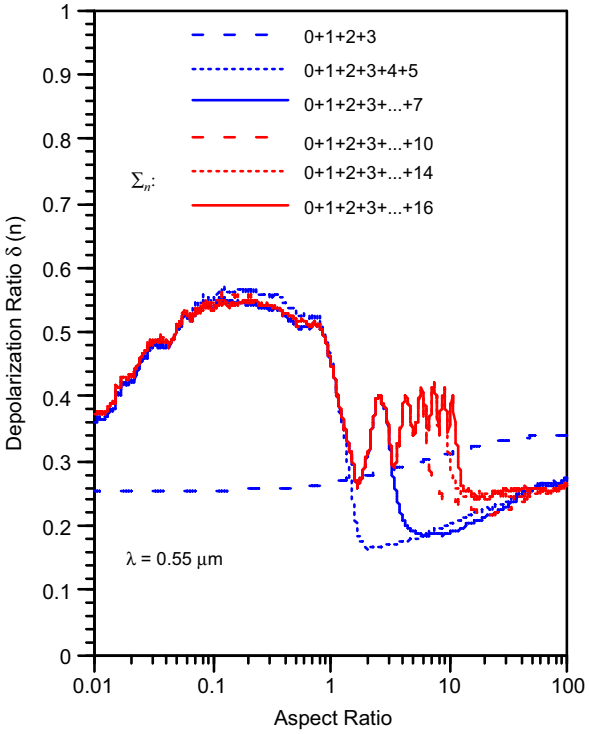

Fig. 10. Backscattering depolarization ratio as a function of the aspect ratio for 3D randomly oriented hexagonal ice columns and plates.

4. Summary

The solution to the scattering of light by randomly oriented hexagonal ice crystals within the framework of the geometric optics method is analyzed in detail. The scattered field is decomposed into the contributions from diffraction and various orders of geometric optics rays. It is shown that the forward and side scattering are mainly from diffraction and lower order rays, and higher order rays have a significant contribution to the scattered field at large scattering angles. The relative weights of the contributions from these rays depend on the aspect ratio.

In this study, we showed that the "V-pattern" variation of the asymmetry factor versus the aspect ratio stems from the dependence of the delta-transmission on the aspect ratio. This mechanism was also well illustrated in the case of the scattering of light by randomly oriented 2D rectangular particles.

Acknowledgements

This study was supported by the National Science Foundation under grant ATM-0239605. We thank H.-M. Cho for assistance in figure preparation.

References

[1] Liou KN. Influence of cirrus clouds on weather and climate process: a global perspective. Mon Weather Rev 1986;114:1167–99.
[2] Stephens GL, Tsay S-C, Stackhous PW, Flatau PJ. The relevance of the microphysical and radiative properties of cirrus clouds to climate and climate feedback. J Atmos Sci 1990;47:1742–53.
[3] Lynch DK, Sassen K, O'C Starr D, Stephens G, editors. Cirrus. New York: Oxford University Press; 2002.
[4] Heymsfield AJ, Iaquinta J. Cirrus crystal terminal velocities. J Atmos Sci 2000;57:916–38.
[5] McFarquhar GM, Heymsfield AJ. Parameterization of tropical cirrus ice crystal size distributions and implications for radiative transfer: results from CEPEX. J Atmos Sci 1997;54:2187–200.
[6] Baum BA, Heymsfield AJ, Yang P, Bedka SM. Bulk scattering properties for the remote sensing of ice clouds. I: Microphysical data and models. J Appl Meteor 2005;44:1885–95.
[7] Baum BA, Yang P, Heymsfield AJ, Platnick S, King MD, Hu YX, Bedka SM. Bulk scattering properties for the remote sensing of ice clouds. II: Narrowband models. J Appl Meteor 2005;44:1896–911.
[8] McFarquhar GM, Yang P, Macke A, Baran AJ. A new parameterization of single-scattering solar radiative properties for tropical anvils using observed ice crystal size and shape distributions. J Atmos Sci 2002;59:2458–78.
[9] Edwards JM, Havemann S, Thelen J-C, Baran AJ. A new parameterization for the radiative properties of ice crystals: comparison with existing schemes and impact in a GCM. Atmos Res 2007;83:19–35.
[10] Ebert EE, Curry JA. A parameterization of ice cloud optical properties for climate models. J Geophys Res 1992;97:3831–6.

[11] Fu Q. An accurate parameterization of the solar radiative properties of cirrus clouds for climate models. J Climate 1996;9:2058–82.
[12] Fu Q, Yang P, Sun WB. An accurate parameterization of the infrared radiative properties of cirrus clouds for climate models. J Climate 1998;25:2223–37.
[13] Fu Q. A new parameterization of an asymmetry factor of cirrus clouds for climate models. J Atmos Sci 2007;64:4144–54.
[14] Neshyba SP, Grenfell TC, Warren SG. Representation of a nonspherical ice particle by a collection of independent spheres for scattering and absorption of radiation: 2. Hexagonal columns and plates. J Geophys Res 2003;108(D15):4448.
[15] Grenfell TC, Neshyba SP, Warren SG. Representation of a nonspherical ice particle by a collection of independent spheres for scattering and absorption of radiation: 3. Hollow columns and plates. J Geophys Res 2005;110:D17203.
[16] Cai Q, Liou KN. Polarized light scattering by hexagonal ice crystals: theory. Appl Opt 1982;21:3569–80.
[17] Takano Y, Liou KN. Solar radiative transfer in cirrus clouds. Part I. Single-scattering and optical properties of hexagonal ice crystals. J Atmos Sci 1989;46:3–19.
[18] Macke A. Scattering of light by polyhedral ice crystals. Appl Opt 1993;32:2780–8.
[19] Hess M, Wiegner M. COP: a data library of optical properties of hexagonal ice crystals. Appl Opt 1994;33:7740–6.
[20] Macke A, Mueller J, Raschke E. Single scattering properties of atmospheric ice crystal. J Atmos Sci 1996;53:2813–25.
[21] Iaquinta J, Isaka H, Personne P. Scattering phase function of bullet rosette ice crystals. J Atmos Sci 1995;52:1401–13.
[22] Baran AJ, Francis PN, Havemann S, Yang P. A study of the absorption and extinction properties of hexagonal ice columns and plates in random and preferred orientation, using exact T-matrix theory and aircraft observations of cirrus. JQSRT 2001;70:505–18.
[23] Baran AJ, Yang P, Havemann S. Calculation of the single-scattering properties of randomly oriented hexagonal ice columns: a comparison of the T-matrix and the finite-difference time-domain methods. Appl Opt 2001;40:4376–86.
[24] Borovoi AG, Grishin IA, Naats E, Oppel U. Light backscattering by hexagonal ice crystals. JQSRT 2002;72:403–17.
[25] Borovoi AG, Grishin IA. Scattering matrices for large ice crystal particles. J Opt Soc Am A 2003;20:2071–80.
[26] Yang P, Liou KN. Single-scattering properties of complex ice crystals in terrestrial atmosphere. Contr Atmos Phys 1998;71:223–48.
[27] Mishchenko MI, Rossow WB, Macke A, Lacis AA. Sensitivity of cirrus cloud albedo, bidirectional reflectance and optical thickness retrieval accuracy to ice particle shape. J Geophys Res 1996;101:16973–85.
[28] Mishchenko MI, Macke A. Incorporation of physical optics effects and δ-function transmission. J Geophys Res 1998;103:1799–805.
[29] van de Hulst HC. Light scattering by small particles. New York: Wiley; 1957.
[30] Hess M, Koelemeijer RBA, Stammes P. Scattering matrices of imperfect hexagonal crystals. JQSRT 1998;60:301–8.
[31] Liou KN. An introduction to atmospheric radiation. 2nd ed. San Diego: Academic Press; 2002.